BIOADHESIVE PATCHES BASED ON CARBOXYMETHYL CELLULOSE/POLYVINYLPYRROLIDONE/BENTONITE COMPOSITES AND SOLUPLUS® FOR SKIN ADMNINISTRATION OF POORLY SOLUBLE MOLECULES

Alessandro Di Michele[a,1], Giulia Fredi[b,c,1], Cinzia Pagano[d]*, Andrea Dorigato[b,c], Paola Calarco[d], Sara Primavilla[e], Fabio Marmottini[f], Maurizio Ricci[d], Alessandro Pegoretti[b,c], Luana Perioli[d]

[a]Department of Physics and Geology, University of Perugia, 06123 Perugia, Italy

[b]Department of Industrial Engineering, University of Trento, via Sommarive 9, 38123, Trento, Italy;

[c]National Interuniversity Consortium of Materials Science and Technology (INSTM), Via G. Giusti, 9 50121 Firenze, Italy

[d]Department of Pharmaceutical Sciences, University of Perugia, Via del Liceo 1, 06123 Perugia, Italy

[e]Istituto Zooprofilattico dell'Umbria e delle Marche, Via G. Salvemini, 1, 06126 Perugia, Italy

[f]Department of Chemistry, Biology and Biotechnology, University of Perugia, 06123 Perugia, Italy

***Corresponding author:** Department of Pharmaceutical Sciences, University of Perugia, Via del Liceo 1, 06123 Perugia, Italy; E-mail address: cinzia.pagano@unipg.it (C. Pagano).

[1]These authors equally contributed to the study.

Published version: https://doi.org/10.1016/j.clay.2021.106377

Abstract

The skin delivery of poorly soluble drugs represents a problem especially for formulations with limited residence time, for which a low amount of drug is released with consequent inefficacy of the therapy. Many purposed approaches suggest the use of nanocarriers as liposomes, micro/nanoparticles or cyclodextrins to solve this problem. This study aims at enhancing the skin delivery of poorly soluble drugs by a simple and scalable formulation. With this aim, a skin self-adhesive flexible and mechanically resistant patch was developed. A composite between sodium carboxymethyl cellulose/polyvinylpyrrolidone and bentonite was prepared and combined to Soluplus®, a co-polymer used to obtain a solid dispersion of poorly soluble drug. With this objective the molecule β-glycyrrhetinic acid (Gly) was used as model. Two different bentonites, having different morphologies (flake-shaped and spherical) and dimensions (micrometric and nanometric), were assayed to evaluate their effect on patch final properties.

Patches containing bentonite/Soluplus® (ratio 1:1 wt./wt.) were the most promising as they feature i) good deformability and suitable mechanical properties to adapt to large deformations during application and use, ii) self-adhesivity to the skin and iii) controlled release. The different morphologies of the chosen bentonites did not produce differences in the final mechanical properties.

The amount of Gly released is able to control the growth of *S. aureus* and Methicillin-Resistant *Staphylococcus aureus*, bacterial strains involved in many skin infections.

Keywords: bentonite composites; sodium carboxymethyl cellulose; poorly soluble molecules; patch; mechanical properties; skin delivery; bioadhesion

1. Introduction

Topical skin disease treatments are often preferable to systemic ones as they avoid many general side effects. In order to make this choice successful, the active ingredient must be adequately formulated. Often traditional topical formulations (gels, creams, foams, solutions and emulsions) show limited efficacy due to the low residence time. Bioadhesive formulations, able to bind the skin and to stay in the application site for a longer time could overcome this problem. Some poorly molecules have been formulated in such systems after inclusion in the hydrophobic cavity of cyclodextrins. Once on skin surface, the active ingredient is released from the complex and empty cyclodextrin remains on skin surface (Jicsinszky and Cravotto, 2020). The limitation in the use of cyclodextrins consists in the risk of their absorption when in the formulation is introduced a penetration enhancer. In fact, it could be responsible for the improvement of cyclodextrins ability to cross the epidermidis with consequent safety problems (EMA, 2017). Another limitation is represented by the limited type of cyclodextrins approved for dermal use, mainly β-CD and e HP-γ-CD at established percentages (Braga 2019), limiting the number of molecules that could be delivered by this carrier. The use of nanotechnologies as nanoemulsions, solid lipid nanoparticles (SLNs), nanostructured lipid carriers (NLCs), liposomes, polymeric nanoparticles and niosomes represents another strategy purposed for the skin delivery of poorly soluble drugs (Ghasemiyeh and Samani, 2020).

Recently the above mentioned technologies have been combined to particular patches, defined microarray patches (Paredes et al., 2021), represented by painless microneedles able to penetrate the epidermidis forming channels by which the drug can reach easily the derma. Despite the proven efficiency, their production is expensive and the scale up is rather difficult. Moreover, carriers as liposomes, SLN and polymer nanoparticles show also stability problems. A suitable formulation must be efficacious and, at the same time, the production scalable and cost-effective (Ghasemiyeh et al., 2020). The scenario of the research in the field of topical application of poorly soluble drugs suggests the need of feasible proposals.

The polysaccharide sodium carboxymethyl cellulose (CMC) is a safe excipient, classified as “generally recognized as safe” (G.R.A.S.), bioadhesive, hydrosoluble and biocompatible and recently considered very useful in wound dressings preparation (Kanikireddy et al., 2020). However, patches based on CMC do not possess suitable resistance to mechanical solicitations (Perioli et al., 2019). To solve this problem, composites

of polymer/inorganic filler can be prepared. Cationic clays are suitable candidates as fillers for this purpose. These materials derive from geologic deposits and have been largely used in many fields (Konta 1995; García-Villén et al., 2020; Borrego-Sánchez et al., 2020). One application is represented by their ability to improve the mechanical properties of polymeric matrices (Adak et al., 2018; Cheikh et al., 2022). Cationic clay minerals show a typical lamellar structure in which the phyllosilicate lamellae (hydrated alumina–silicates) host cationic species (e.g. Na^{+}, Ca^{2+}, Mg^{2+}) between their interlamellar spaces. These materials show many properties such as high specific surface area, adsorption capacity, swelling capacity (Massaro et al., 2018; Ryu et al., 2020) making them useful in health field for many applications e.g. rheological agent, solid emulsifier, carrier for drugs (Ghadiri et al., 2015). Bentonite (Bent) is one of the most used clay minerals in pharmaceutical field due to its versatility, biocompatibility and low costs (Peña-Parás et al., 2018). Bent is a 2:1 type aluminosilicate (Guo et al., 2018) belonging to smectite group of clay minerals. Bent demonstrated to be a suitable filler for polymeric matrices (Devi and Dutta, 2017; Alekseeva et al., 2019; Osman et al., 2020) and for this reason chosen for this research to improve the mechanical properties of the developed patches.

This paper has the objective to develop and characterize autoadhesive polymeric patches for the topical application of poorly soluble molecules and the strategy was developed with industrial scalability in mind. The planned formulations were based on the realization of composites based on sodium carboxymethylcellulose (CMC) and Bent. In order to allow a complete release of poorly soluble drugs the co-polymer Soluplus® (SL) was introduced in patch composition. SL (polyvinyl caprolactam and polyvinyl acetate) is a graft copolymer of polyethylene glycol (PEG), developed to improve the solubility of poorly soluble drugs amorphized by the formation of solid dispersions (Shamma and Basha, 2013; Al-Zoubi et al., 2018; Barmpalexis et al., 2018; Shi et al., 2018; Solanki et al., 2018) stabilizing them by preventing the recrystallization (Dian et al., 2014; Tsinman et al., 2015). Moreover, once in contact with water, SL is able to form micelles in which poorly soluble molecules can be stored improving their solubility (Zeng et al., 2017). SL is a safe excipient as testified by the studies performed according to the Organisation for Economic Cooperation and Development (OECD, guidelines for acute toxicity, irritation, and sensitization). SL has been largely used for oral dosage forms (Pignatello and Corsaro, 2019; Tian et al., 2020; Giri et al., 2021) however, it represents a promising excipient

to be used also for topical products. In this research SL was used in order to modify the solid state of the loaded active ingredient with the aim to allow a complete release from the formulation.

This study has the aim to optimize the most suitable CMC/Bent composite composition combined to SL in order to obtain a bioadhesive patch showing suitable mechanical properties and, at the same time, able to favour the complete release of the poorly soluble molecules. In this study β-glycyrrhetinic acid (Gly) was used as model drug.

2. Materials and Methods

2.1. Reagents

Bent (sodium montmorillonite), sodium montmorillonite nanoclay (Nanomer® PGV) (furnisher datasheets), and absolute ethanol (EtOH abs) were purchased from Sigma Aldrich (Milano, Italy). Sodium carboxymethyl cellulose (CMC, viscosity 2% 400-600 mPa·s), 18-β-glycirrethinic acid (Gly) and glycerol were supplied by A.C.E.F. s.p.a., Fiorenzuola d'Arda (Piacenza, Italy). Polyvinylpyrrolidone (PVP K90, density = 1.2 g/ cm^3, M_w = 1,300,000 Dalton) was supplied by ISP (Baar, CH-Switzerland). Soluplus® (SL, polyvinyl caprolactame-polyvinyl acetate-polyethylene glycol graft copolymer, M_w = 118,000 g/mol, density 1.082 g/cm^3) was a gift from BASF (Ludwigshafen, Germany). Ultrapure water was obtained by reverse osmosis process by a MilliQ system Millipore (Milano, Italy). Other reagents and solvents were of analytical grade and used without further purification. Simulated wound fluid (SWF) pH 6.5 was prepared by dissolving 8.30 g of NaCl and 0.28 g of $CaCl_2$ in 1000 ml of ultrapure water (Pagano et al., 2019). Buffered peptone water: deionized water 1000 ml, buffered peptone water (Biolife Italia, Monza, Italy) 20 g. Blood Agar with 5% Sheep Blood: deionized water 1000 ml, Columbia Agar Base (Microbiol) 44 g, Sheep Blood Defibrinated (Allevamento Blood di Fiastra Maddalena, Icribis, Milano, Italy) 50 ml. Bacterial suspension, from IZUM collection, was used at a known concentration of $1x10^3$CFU/ml for the antimicrobial test.

2.2. Patches preparation

Patches were obtained by solution-blending method (Guo et al., 2018) properly modified. The hydrogels having the compositions reported in Table 1 were prepared as follows: CMC, PVP K90, SL and Bent (when used) were mixed by mortar and pestle then glycerol was added. Finally, water was added gradually under mixing in order to induce hydrogel formation. The air incorporated during the preparation was removed by a THINKY ARE-

250 mixer (2000 rpm, 5 min, room temperature R.T.). Loaded patches were prepared mixing Gly (0.1% w/w) CMC, PVP K90 by mortar and pestle, SL and Bent (when used). Then glycerol was added and finally water in order to induce hydrogel formation. The hydrogels (3.5 g) were casted in circular silicon moulds (r = 1.5 cm) and placed in oven at 37.0°C for 24 h.

2.3. Thermal analyses

Thermogravimetric analysis (TGA) was carried out by a Q5000IR thermobalance (TA Instruments, Inc., New Castle, DE, USA). Specimens of approx. 8 mg were tested at a heating rate of 10°C/min up to 700°C, under a nitrogen flow of 10 ml/min. The test allowed the measurement of the water content by calculating the mass loss at 120°C, the degradation temperature (T_d), intended as the peak of the mass loss derivative signal, and the residual mass after the test. Differential scanning calorimetry (DSC) tests were performed on 50% relative humidity (R.H.) conditioned samples by using a Mettler Toledo DSC30 calorimeter. Each sample was put in aluminum crucibles with a volume of 40 µl and tested under a nitrogen flow of 100 ml/min, heating/cooling rate of 10°C/min. Two consecutive heating cycles from -50 up to 180°C were performed. In the first cycle the presence of water can be identified by a broad endothermic peak related to water evaporation, whereas in the second one the glass transition temperature (T_g) of the Na-CMC matrix can be better measured. The water weight fraction was calculated by dividing the enthalpy of the endothermic peak by the enthalpy of evaporation of water (2260 J/g).

2.4. Nitrogen adsorption–desorption isotherms

The measurement of nitrogen adsorption–desorption isotherms was performed by Micromeritics ASAP 2010 instrument working at −196.15°C. Before the analysis the samples were outgassed for 48 h at R.T. The Brunauer, Emmett, and Teller (B.E.T.) method was used to calculate the specific surface area of the samples analysed.

2.5. Dimensional analysis

The dimensional analysis of Bent was performed by SPOS technique (Single Particle Optical Sensing) using an Accusizer C770 (PSS Inc., Santa Barbara, CA), n=3 ±SD. The polydispersion was calculated according to Eq. 1:

$$Span = \frac{Dv_{0.9} - Dv_{0.1}}{Dv_{0.5}} \qquad \text{(Eq. 1)}$$

Where: $D_{0.1}$, $D_{0.5}$ and $D_{0.9}$ are the size values corresponding to cumulative distributions at 10%, 50% and 90%, respectively and represent the particle sizes below which (10%, 50% and 90%, respectively) the samples belong.

2.6. SEM and TEM analyses

Bent morphology as well as patches surface morphology and thickness were studied by Field Emission Scanning Electron Microscopy (FE-SEM LEO 1525 ZEISS) using an electron high tension of 5 and 15 kV. Small pieces of sample were cut and mounted on stubs with double sided adhesive carbon tape and metalized with chromium (8 nm). The images were obtained using secondary electron (SE) and In-lens detectors at magnifications of 500X and 5000X.

TEM analysis on Bent was performed by a Trasmission Electron Microscope (TEM) Philips EM 208.

2.7. Mechanical analysis

Tensile tests were performed on patches conditioned at 50% RH with a universal dynamometer Instron 5969 (Instron, Norwood, MA, US) equipped with a 10 N load cell. Specimens with nominal in-plane dimensions of 30 x 5 mm^2 were cut from the provided patches and mounted on paper frames to ease handling. The initial distance between the grips was 20 mm and the tests were performed at a testing speed of 10 mm/min. Five specimens were tested for each composition. The test allowed the calculation of the secant moduli at strain values of 5%, 25% and 50% ($E_{5\%}$, $E_{25\%}$, $E_{50\%}$), and of the stress and the strain at break (σ_b and ε_b). Creep tests were performed at 30°C with the TA DMA Q800 (TA Instruments, Inc., New Castle, DE, US) equipped with a 16 N load cell. Rectangular specimens with nominal in-plane dimensions of 30 x 5 mm were cut out of the prepared patches, mounted on the instrument with a gauge length of 10 mm (calculated as the distance between the grips). A constant stress of 22 kPa, corresponding to the 30% of the tensile strength of the neat unloaded matrix (H-CMC_S_1), was applied for 60 min and the recorded displacement was used to calculate the creep compliance, determined as the ratio between the measured strain and the constant stress, as a function of time.

2.8. X-ray diffraction (XRD)

X-Ray Diffraction (XRD) data were collected by an Italstructures IPD3000 diffractometer equipped with a Co anode source (line focus), a multilayer monochromator to suppress k-β radiation and fixed 100-μm slits. Samples were positioned in reflection geometry with a 5° angle with respect to the incident beam; the reference drug sample was loaded in a standard powder holder, whereas prepared patches were positioned on a zero-diffraction

Si wafer. Powder patterns were collected by means of an Inel CPS120 detector over 5-120° 2θ range (0.03 degrees per channel) with a total acquisition time of 1800 seconds for each sample. Patch samples were tested both after conditioning at 50% RH and after drying at 80°C for 12 h. Dried samples gave better results in terms of signal-to-noise ratio (S/N), but no additional peaks could be detected. Therefore, only the results of the dried samples are presented.

2.9. Ex vivo adhesion studies

Patch ex vivo adhesion capacity was evaluated using pig skin samples (from shoulder region), obtained from Large White pigs weighing ~165–175 kg, furnished by Veterinary Service of ASL N. 1 Umbria, Città di Castello (Perugia, Italy) and used within 12 h from pig death (Perioli et al., 2004). The ex vivo adhesion force was measured by a dynamometer (Didatronic, Italy). The patch was attached on a support, connected to the dynamometer, using a cyanoacrylate glue. A piece of porcine skin tissue was fixed with cyanoacrylate glue on the surface of a glass support placed in a thermostatic bath at 32.0°C ± 0.5. Every patch was cut in squares of 2 x 2 cm. The free side of the patch was wetted with 100 µl of SWF and put in contact with the skin sample by applying a light force for 1 min. The force necessary for patch detachment from skin was measured and expressed as average of three measurements (n= 3).

2.10. FT-IR analysis

FT-IR spectra were recorded between 400-4000 cm^{-1} by a Shimadzu IR Spirit QATR-S spectrometer.

2.11. Gly content in loaded patches

Each patch (1 x 1 cm) was weighted, placed in a flask containing 5 ml of an EtOH/SWF (50/50 v/v) solution, stirred at 600 rpm for 24 h at R.T. Gly content in the samples was measured spectrophotometrically as described in par. 2.13.

2.12. In vitro release studies

Gly release from loaded patches was evaluated by vertical Franz diffusion cell (USP <1724> PermeGear, Inc., Bethlehem, PA, USA, diameter 20 mm). A cellulose membrane (Whatman 41, Whatman GmbH, Dassel, Germany) was placed between the two chambers. As receptor medium (15 ml) a solution of EtOH/SWF (50/50 v/v), thermostated at 32.0 ± 0.5°C and magnetically stirred (600 rpm), was used. The patch (circle of 3.14 cm^2) was placed on top of the cellulose membrane (donor chamber). The donor medium was represented by 2 ml of

EtOH/SWF (50/50) solution. All openings including donor top and receptor arm were sealed with parafilm® to prevent solvent evaporation. Samples (500 µl) were withdrawn at established times from the receiving phase and replaced with the same volume of EtOH/SWF (50/50) solution. Gly amount in each sample was measured spectrophotometrically as described in par. 2.13.

2.13. Gly quantitative analysis

Gly quantification was carried out by UV–vis spectrophotometry (UV–Visible Agilent model 8453). The amount of Gly in each sample was accomplished using a standard curve constructed in EtOH/SWF (50/50 v/v) (λ_{max}=252.0 nm, R^2=0.99). All experiments were performed in triplicate, each result represents an average of three measurements and the error was expressed as standard deviation (± SD).

2.14. Antimicrobial activity assay

The antibacterial activity of Gly released from the developed patch was studied on *S. aureus* and methicillin-resistant (MRSA) strains. The stored strains were revitalized on Brain Heart Infusion Broth and incubated according to their growth conditions *S. aureus* at 37.0°C for 24 ± 2 h and MRSA at 37.0°C for 24-48 h. The experiments were performed using the protocol suggested by Oyama et al. 2016 properly modified (Oyama et al., 2016). The cultural media, Buffered Peptone Water and Blood Agar, were prepared according to the recipe previously described (see Materials). Buffered peptone water (900 µl) was poured into culture multiwell plate and 100 µl of bacterial suspension was added reaching a final concentration of $1x10^3$ CFU/ml (n=3 for each strain tested) then incubated with the patch (1 x 1 cm^2) at 37.0°C. The untreated bacterial suspension was used as a control. The bacteria growth was evaluated after 6 and 24 h of incubation. A set of serial dilutions was made from each sample in order to determine the number of CFU, 100 µl were spread onto Blood Agar Petri dishes and the colonies were counted after 24 h of incubation at 37°C. The number of CFU was calculated in accordance with the ISO 7218:2007 standard according to equation 2 (Eq. 2):

$$N = \frac{\Sigma C}{V\ x\ 1.1\ x\ d} \qquad Eq.2$$

where C is the sum of the colonies counted on the two dishes from two successive dilutions, V is the volume of inoculum placed in each dish (ml), d is the dilution corresponding to the first dilution retained.

3. Results and Discussions

3.1. Patch preparation and characterization

Patches were prepared by casting method starting from hydrogels which composition was optimized referring to a previous study (Pagano et al., 2020), using NaCMC (3%) and PVP K90 (0.1%) as bioadhesive polymers (Kurakula and Rao, 2020; Ugoeze, 2020). In order to improve the mechanical properties, the filler Bent, already used for such purpose (Guo et al., 2018) was introduced in the composition. In particular two different Bent were used, one micrometric (hereinafter called BE) and the other one nanometric (hereinafter called NC).

XRD patterns of the two Bent (Fig. 1S) were analysed by the DIFFRAC.EVA (Bruker) and the Crystallography Open Database software was used in order to know their crystalline phase composition. A Rietveld refinement procedure was applied for phase quantification using the TOPAS6 (Bruker) software. The main crystalline phases identified for BE were: quarz (SiO_2, 2%), albite ($NaAlSi_3O_8$, 19%), illite ($K_{0.65}Al_{2.0}[Al_{0.65}Si_{3.35}O_{10}](OH)_2$, 34%) and montmorillonite $(Na,Ca)_{0.33}(Al,Mg)_2(Si_4O_{10})(OH)_2.nH_2O$, 45%) as observed from other authors (Vipulanandan & Mohammed, 2020). For NC the following composition was found: montmorillonite 49%, illite 42%, albite 8%, quartz 1%.

By SEM analysis emerged that the two Bent display different morphologies. In particular, BE shows an irregular flake-shaped structure (Fig. 2SA) typical of montmorillonite clays while NC shows particles with spherical morphology and smooth surface (Fig. 2SB) probably attributable to the treatment to which montmorillonite was submitted to obtain the nanoclay form. TEM analysis allowed to better distinguish the NC nanometric particles (Fig. 2SD) compared to BE (Fig. 2SC). BE and NC were then characterized in terms of thermal properties and specific surface area. The TGA analysis showed a water content of 5.8% wt./wt. and 13.1% wt./wt. for BE and NC, respectively. The analysis of the specific surface area showed a value of 30.7 ± 0.1 m^2/g for BE, ascribable to the particles irregular surface and 18.6 ± 0.1 m^2/g for NC. Dimensional analysis performed by SPOS technique showed similar values for the two Bent, mode = 9.47 ± 0.12 μm and 10.55 ± 0.20 μm for BE and NC respectively. In the case of NC, it is reasonable to think that the nonometric particles form aggregates (as detectable in the micrograph reported in Fig. 1SB) responsible for the obtained results. In the case of BE, a high polydispersion degree was measured (Span= 1.57 ± 0.02 *vs* 1.25 ± 0.05 for BE and NC respectively), probably due to the presence of small particles as detectable in the corresponding micrograph (Fig. 1SA).

Taking into account the dimensional and morphological differences of the two different Bent, the influence of these properties on patch mechanical properties was investigated. In order to do this, hydrogels with different

BE and NC amounts (0.5, 0.6, 0.7, 0.8, 0.9, 1% wt.) were prepared and used for patch preparation. After a preliminary evaluation, the most interesting percentages resulted 0.5% wt./wt., 0.7% wt./wt. and 1% wt./wt (Table 1). The thermal analysis, performed by TGA and DSC, showed a residual mass (~10%) for all the samples due to the inorganic residue of Bent. By TGA a water loss of ~22.0% ± 2.14 was observed suggesting that the two different Bent (BE and NC) did not influence patches thermal profiles (Table S1).

From DSC analysis it is detectable that the T_g increases when Bent are introduced in the patch (CMC_S_0 < CMC_BE_1 and CMC_NC_1), confirmed also from literature data (Dorigato et al., 2011). However, for all samples no linear trend is detectable between the increase of Bent percentage and T_g value increase as the samples containing intermediate percentages of Bent (0.5 and 0.7%) also contain SL, which could influence the T_g values. Subsequently patch surface morphology and thickness were measured by SEM analysis; these properties are very important as these formulations were projected to be applied on the skin. The patch prepared without Bent (CMC_S_1) shows a surface rather smooth and continuous (Fig. 3SA). Increasing the magnification, small pores can be detected (Fig. 3SB) highlighting a sponge-like appearance attributable to SL presence in the composition. This observation is confirmed observing patch CMC_S_0, prepared using only CMC (without SL), resulting compact with a continuous surface (Fig. 3SC and 3SD). The introduction of Bent in patch compositions is responsible for the morphological modifications as a wrinkled surface is detectable in all cases with clear differences between BE and NC (Fig. 1 A-H).

The use of high BE amounts (patch CMC_BE_1) is responsible for a non-homogeneous dispersion in the polymeric matrix (Fig. 1A) and the presence of aggregates can be detected (Fig. 1B). Decreasing BE content, the distribution become more homogeneous, but the presence of aggregates is still present especially for patch CMC_BE_0.7 (Fig. 1C and 1D). Patch CMC_BE_0.5 resulted the most homogeneous without the presence of aggregates (Fig. 1E and 1F). NC dispersion in the polymeric network in more uniform than BE even the presence of aggregates is also observable for the patches containing high amounts: CMC_NC_1 (Fig. 1G and 1H), CMC_NC_0.7 (Fig. 1I and 1L) while CMC_NC_0.5 is the most homogeneous (Fig. 1M and 1N). Also patch thickness was measured by SEM analysis (Table 2). Comparing patch CMC_S_1 (containing both CMC and SL) with patch CMC_S_0 (containing only CMS), the latter is thicker probably due to the higher CMC content. Moreover, patch CMC_S_0 results more compact compared to patch CMC_S_1. As expected, the introduction

of Bent in patch compositions is responsible for thickness increase compared to CMC_S_1. In the case of patches containing BE the obtained values (Table 2) suggest that the different thickness measured are not attributable only to BE content as an effect due to SL content can be detected. Patch CMC_BE_0.5, containing the highest SL amount, showed a sponge-like morphology responsible for the high thickness measured despite the low BE amount. On the other hand, patches containing high BE % result very compact and the thickness increases as BE amount increases (patch CMC_BE_0.7 < patch CMC_BE_1, Table 2).

Patches containing NC showed different characteristics compared to the other kinds. The thicknesses measured are comparable to each other (Table 2), only patch CMC_NC_1, containing the highest amount of NC and without SL, is very compact and thin. Also, in this case the sponge-like structure is detectable for patches containing the highest SL amount namely CMC_NC_0.7 and CMC_NC_0.5. In the case of patches containing BE, thickness increases as the content increase; it decreases from 0.5 to 0.7 and increases from 0.5 to 1 in the case of NC.

3.1.2. X-ray diffraction analysis (XRD)

Bent is a material largely used as filler to improve the mechanical properties of polymeric matrices. It forms composites with polymers in which they are dispersed and/or exfoliated (Zhu et al., 2019). In order to better understand the form of Bent once in the polymeric matrix, XRD analysis was carried out. Patches XRD patterns (Fig. 2) do not show the typical diffraction peaks observed for the raw BE and NC (Fig. 1S) suggesting that these could be dispersed in the polymeric network or exfoliated as observed from other authors (Bochek et al., 2011). Moreover, all the samples have a broad peak for values of 2θ near 24°, due to the short-range order present in the amorphous matrix (Saha and Dey Ray, 2013; Xu and Zhang, 2015). Also, low intensity peaks at 2θ values below 10° and above 60° are present due to sample geometry effects (sample not perfectly planar) or signals from the silicon substrate.

3.1.3. Mechanical analysis

The following parameters were measured for each patch: i) elastic modulus at deformation of 5% ($E_{5\%}$), 25% ($E_{25\%}$) and 50% ($E_{50\%}$); ii) stress at break (σ_b) and iii) deformation at break (ε_b). The obtained results (Table 2) show that the values of $E_{5\%}$, $E_{25\%}$ and $E_{50\%}$ increase up to 1% of Bent content confirming the strong dependency of material stiffness on filler aggregation as highlighted in recent studies (Dorigato et al., 2013, Dorigato et al.,

2017). According to these, filler aggregation may constrain a portion of matrix limiting the macromolecules mobility and providing a stiffening effect. σ_b values are increased in samples containing 1% of Bent compared to that of the sample without them. The deformation ability is an important property of a patch that should be applied on skin. It is noteworthy that skin surface is not always regular and, depending on the application site, it is susceptible to deformations due to the movements. Since SL decreases the secant moduli values (Table 2), it gives a positive contribution in decreasing patch stiffness, as this makes the patches more compliant to skin's movements and likely more comfortable during use. In accordance to tensile tests a decrease in the creep compliance (deformation under load with time) values at 60 min is observed for the samples containing 1% of both BE and NC due to the stiffening effect of the filler. From creep compliance results, considering the patches containing micrometric Bent (BE), CMC_BE_0.5 showed the best values. In the case of patches prepared with NC (CMC_NC_0.5 and CMC_NC_0.7) CMC_NC_0.5 was selected as showed the most suitable deformation at break (ε_r) value. Table 2 also shows nearly no differences between patch CMC_BE_0.5 and CMC_NC_0.5, suggesting that Bent morphology does not substantially influence the mechanical properties using a filler content of 0.5% wt. For this reason patches CMC_BE_0.5 and CMC_NC_0.5 were submitted to the next studies.

3.2. Loaded patches preparation and characterization

CMC_BE_0.5 and CMC_NC_0.5 were loaded with the model drug Gly (0.1% wt.), following the procedure described in method section (par. 2.2.) and then characterized. Patches CMC_BE_1 and CMC_NC_1 were prepared as well and used for comparison. Firstly, the exact Gly amount for area unit was measured as described in par. 2.11 obtaining a content of ~0.4 mg/cm^2 (Table 3).

3.2.1. Thermal analysis of loaded patches

The TGA results are reported in Table 3. The matrix degradation temperature is not significantly influenced by the composition. The water content is slightly higher for the samples containing NC and it decreases slightly when the filler content increases. The water evaporation enthalpies allowed an estimation of the weight fraction of water (Table 3, Fig. 4S) which range between 27 wt% and 30 wt%. The T_g is higher for the samples containing BE than for those containing NC and decreases when the filler content increases.

3.2.2. Mechanical analysis of loaded patches

The results of the quasi-static tensile tests are reported in Fig. 3. Representative stress-strain curves (Fig. 3A) evidence a similar tensile behaviour for the four compositions, with the stress increasing with strain until a maximum load, after which the samples break suddenly into two pieces and the stress drops to zero. For the samples containing BE the elastic moduli (Fig. 3B) increase with the filler weight fraction, while the opposite trend is observed for the samples containing NC, even though for these samples the difference in stiffness is smaller. Patch CMC_BE_1 is the sample showing the highest elastic moduli values. Moreover, as the stress increases with strain until failure, the composition showing the highest strain at break (i.e. patch CMC_NC_0.5) is also that having the highest stress at break (Fig. 3C). Finally, the results of the creep tests are reported in Table 3. Creep compliance values decrease as filler content increases for both for the samples containing BE and NC. The sample with the lowest creep compliance is patch CMC_BE_1, that presenting the higher stiffness (determined in quasi-static tensile tests). Comparing the creep compliance values between loaded and unloaded patches (Table 3), it was observed that the presence of Gly in the composition increases this value. The highest results were obtained for patches CMC_BE_0.5 and CMC_NC_0.5 and thus chosen and used for the next studies.

3.2.3. Morphology and thickness of loaded patches

The morphological analysis performed on the selected patches showed in both cases a wrinkled surface due to Bent particles dispersed in the polymeric matrix (Fig. 5S). SEM micrographs obtained by back-scattered electron detector allowed to observe the particles of the fillers dispersed in the polymeric matrix (Fig. 6S). In particular, in the case of CMC_BE_0.5 Gly it is possible to detect BE particles (Fig. 6SA) resulting of higher dimensions than CMC_NC_0.5 Gly, containing the nanoclay form (Fig. 6SB).

Patch thickness resulted increased only for CMC_NC_0.5 Gly (0.6875 ±0.013 mm) compared to the unloaded one (0.3422 ± 0.042, Table 2). Observing the obtained micrograph (Fig. 5SD) it is possible to observe the presence of pores responsible for the important thickness increase observed.

For CMC_BE_0.5 Gly the measured value is comparable to the unloaded (0.4633 ±0.020 mm *vs* 0.4704 ± 0.012 mm for CMC_BE_0.5 Gly and CMC_BE_0.5 respectively). In fact, in the corresponding micrograph (Fig. 5SB) no pores are detectable, resulting more compact than patch CMC_NC_0.5 Gly.

3.2.4. Ex vivo adhesion studies

The patches were developed to adhere to skin without the need of adhesives. Thus, the bioadhesion capacity, intended as force necessary for patch detachment from skin tissue was studied as well. The obtained results showed an adhesion force of 0.32 ± 0.04 N and 0.18 ± 0.02 N for patches CMC_NC_0.5_Gly and CMC_BE_0.5_Gly respectively. The differences could be ascribed to the different availability of groups able to bind skin surface. In order to better understand this aspect, FT-IR analysis was performed (Fig. 4). Gly spectrum shows the typical peaks at 1704 and 1664 cm^{-1} due to carboxylic acid and carbonyl moieties vibrations (Sui et al., 2020). CMC shows a broad absorption band centred at 3300 cm^{-1} due to the stretching frequency of –OH groups, a band at 1592 cm^{-1} attributable to $–COO^-$ asymmetric stretching and another at 1426 cm^{-1} due to symmetric stretching of $-COO^-$. The band at 1047 cm^{-1} is attributable to C-O stretching (Demirci et al., 2020). Glycerol shows a strong band at 3300 cm^{-1} due to -OH stretching, two bands at 2880 and 2900 cm^{-1} attributable to CH stretching. A peak at 1034 cm^{-1} due to C-O stretching (Salehpour and Dubé, 2012). SL spectrum shows a band at 1625 cm^{-1} due to C(O)N or amide group and another at 1725 cm^{-1} due to $OC(O)CH_3$ or ester group (Lan et al., 2010). Moreover two detected peaks at 2927 and 2857 cm^{-1} can be due to asymmetric and symmetric CH stretching (Lin et al., 2015). NC and BE show a peak at 3600 cm^{-1}, attributable to stretching vibration of -OH groups, a band centred at 3360 cm^{-1}, due to the stretching vibrations of –OH structural groups. The bands at 915 and 849 cm^{-1} are attributable to bending vibrations of Al-Al-OH and Al-Mg-OH, respectively. A peak at 1633 cm^{-1} is detectable as well due to H-O-H bending (Peng et al., 2020). The loaded film shows the typical peaks of glycerol. The peaks at 1633 cm^{-1} and 3600 cm^{-1} (NC, BE) and those of Gly at 1704 and 1664 cm^{-1} are not detectable suggesting that Bent interact with Gly establishing probably hydrogen bonds.

The nanoclay (NC), once dispersed in the polymeric network should expose a high surface area able to bind more Gly molecules than patch containing BE. The higher binding degree between NC and Gly makes Bent less available to establish interactions with CMC. This means that CMC possesses a high number of sites available to interact with skin surface making CMC_NC_0.5 Gly more bioadhesive than patch CMC_BE_0.5 Gly.

3.2.5. Release study

The in vitro studies showed that Gly is released from the patches by a sustained mechanism, observing different profiles in the two tested formulations (Fig. 5). In the case of CMC_BE_0.5 Gly a faster release can be detected during the first 6 h (~57% of Gly released), reaching ~65% after 24 h and ~ 68% after 48 h. However the release

is incomplete until the end of the experiment. Patch CMC_NC_0.5 Gly released the active ingredient slowly (~38% in 6 h) increasing to 83% and 95% at 24th h and 48th h respectively.

In order to better understand the differences observed and the kinetic mechanisms involved in Gly release from the two patches, the in vitro release data were processed by the following mathematical models: zero-order, first-order and Higuchi (Ritger and Peppas 1987; Siepmann et al., 2011). The zero-order model describes a kinetic in which the release rate is independent from the active ingredient concentration. When the release rate is dependent from the concentration the process is described by the first-order model. The Higuchi model describes a kinetic driven by Fickian diffusion (time-dependent). The obtained results (Table 4) show the best fitting (R^2 = 0.88) for Higuchi model in the case of patch CMC_BE_0.5 Gly suggesting that the diffusion is the main mechanism driving Gly release from the patch. Thus, the polymeric network seems to be able to control Gly diffusion in the bulk together to BE dispersed in the matrix. In the case of patch CMC_NC_0.5 Gly the best fitting (R^2= 0.96) was obtained for the first order kinetic suggesting that in this case the release is concentration dependent. As this patch releases a lower Gly amount in the first 6 h, in comparison to patch CMC_BE_0.5 Gly, it was necessary to perform a further characterization in order to explain the differences. Thus, we decided to investigate Gly solid state in the patch by XRD analysis. The obtained patterns (Fig. 7S) show in both cases the lack of typical sharp peaks of Gly crystalline domains. Even the broad halos present on the spectra of all patches, imputable to amorphous or nanocrystalline phases, does not seem to be compatible with the peaks of the solid drug and it is probably attributable to the other phases in the CMC matrix. XRD did not show substantial differences of Gly state between the two formulations. Thus, it was hypothesized that the observed differences are attributable to the different organization of the two Bent dispersed in the polymeric matrix as well as to the different interaction with Gly molecules. In fact, it is reasonable to think that in the case of CMC_NC_0.5 Gly, the nanoclay (NC) is dispersed exposing a high surface area available to establish interactions (as detected by FT-IR analysis) with Gly molecules. This brings to a higher binding degree between Gly molecules and NC (in CMC_NC_0.5 Gly) compared to Gly/BE (CMC_BE_0.5 Gly), responsible for the different release profiles observed (Fig. 5). In fact, during the first 6 h Gly release from patch CMC_NC_0.5 Gly is lower than CMC_BE_0.5 Gly due to the energy required for Gly-NC binding breaking. At 24th h the amount of Gly released from patch CMC_NC_0.5 Gly increases resulting almost complete at 48th h. In the case of patch CMC_BE_0.5

Gly, the amount released within the first 6 h is higher compared to patch CMC_NC_0.5 Gly probably because in this case many Gly molecules are free to diffuse through the polymeric network. It must be highlighted that at 24th h Gly concentration reaches a plateaux of ~ 60%, that can be explained considering that at this time point the equilibrium of Gly concentration between the patch and bulk solution was obtained with consequent interruption of the diffusion mechanism.

3.2.6. Antimicrobial activity assay

The antimicrobial activity of the prepared patches CMC_BE_0.5 Gly and CMC_NC_0.5 Gly was observed against *S. aureus* and MRSA strains sensitive to Gly (Pellati et al., 2009; de Breij et al., 2016; Oyama et al., 2016). The obtained results (Table 5, Fig. 8S) showed that both patch CMC_BE_0.5 Gly and patch CMC_NC_0.5 Gly release a Gly amount effective against *S. aureus* and *MRSA* within 6 h. *S. aureus* demonstrated to be the most sensitive as testified by the values measured. After 6 h the control (untreated bacteria) Log CFU/ml of 6.51 shifted to 4.45 and 3.71 for patches CMC_BE_0.5 Gly and CMC_NC_0.5 Gly respectively. After 24 h, the Log CFU/ml calculated was 7.04 and 6.20 for patches CMC_BE_0.5 and CMC_NC_0.5 respectively *vs* 7.93 of control. Also *MRSA* resulted sensitive to the patches. After 6 h the control CFU/ml of 5.62 shifted to 4.90 for patch CMC_BE_0.5_Gly and 4.86 for patch CMC_NC_0.5_Gly.

The same experiment was performed on the unloaded patches, CMC_BE_0.5 and CMC_NC_0.5, in order to evaluate the possible contribution of Bent to the observed antimicrobial activities. The obtained results (Table S2) highlighted no activity of empty films.

4. Conclusions

Patches based on carboxymethyl cellulose/polyvinylpyrrolidone/ Bent composites combined with the co-polymer Soluplus® were prepared and characterized. The studies performed highlighted that 0.5% wt./wt. is the best amount of Bent to be used in order to obtain a formulation with suitable mechanical properties. This % does not produce substantial differences in the mechanical properties changing Bent morphology. For example, the deformation at break resulted ε_r = 383 ± 53 MPa and 404 ± 53 MPa for patches CMC_BE_0.5 and CMC_NC_0.5 respectively. The introduction of Soluplus® in patch composition demonstrated to reduce Gly crystallinity making it ready to be released from the formulation. Moreover, it was observed that Soluplus® is able to reduce patch stiffness obtaining a formulation more adaptable to skin and comfortable during the use.

In conclusion patches containing Bent/Soluplus® in the ratio 1:1 showed all the desired properties as i) deformability to resist to solicitations during and after application, ii) self-adhesivity to the skin without use of glues, iii) controlled release capacity useful to obtain an efficacious treatment during 48 h by a single application and iv) easy removal by washing due to the hydrophilicity of the components used. In consideration of this, it is possible to state that the purpose of the work has been fully achieved and a useful, effective and easily usable device has been developed.

In addition to this, it is important to underline that the raw materials used are readily available and cheap and that the proposed production process is scalable.

Declaration of Competing Interest

The authors declare no conflict of interest.

Acknowledgement

Authors sincerely acknowledge Prof. Riccardo Vivani from the Department of Pharmaceutical Sciences for Rietveld refinement of XRD, Mr. Marco Marani from the Department of Pharmaceutical Sciences for technical assistance. Authors are grateful to Dr. Simonetta De Angelis from ASL N. 1 Umbria (Città di Castello, Perugia, Italy) for providing pig skin samples.

References

Adak, B., Butola, B.S., Joshi M., 2018. Effect of organoclay-type and clay-polyurethane interaction chemistry for tuning the morphology, gas barrier and mechanical properties of clay/polyurethane nanocomposites. Appl. Clay Sci. 161, 343-353.

Al-Zoubi, N., Odah, F., Obeidat, W., Al-Jaberi, A., Partheniadis, I., Nikolakakis, I., 2018. Evaluation of Spironolactone Solid Dispersions Prepared by Co-Spray Drying With Soluplus® and Polyvinylpyrrolidone and Influence of Tableting on Drug Release. J. Pharm. Sci. 107(9), P2385-2398.

Alekseeva, O. V., Rodionova, A.N., Bagrovskaya, N.A., Agafonov, A. V., Noskov, A. V., 2019. Effect of the bentonite filler on structure and properties of composites based on hydroxyethyl cellulose. Arab. J. Chem. 12(3), 398-404.

Barmpalexis, P., Karagianni, A., Kachrimanis, K., 2018. Molecular simulations for amorphous drug formulation: Polymeric matrix properties relevant to hot-melt extrusion. Eur. J. Pharm. Sci. 119, 259-267.

Bochek, A.M., Zabivalova, N.M., Yudin, V.E., Gofman, I.V., V. K. Lavrent'ev, Volchek, B.Z., Vlasova, E.N., Abalov, I.V., Brusilovskaya, N.G., Osovskaya, I.I. 2011. Properties of Carboxymethyl Cellulose Aqueous Solutions with Nanoparticle Additives and the Related Composite Films. Polym. Sci. 53(12) 1167-1174.

Borrego-Sánchez, A., Viseras, C., Sainz-Díaz, C.I., 2020. Molecular interactions of praziquantel drug with nanosurfaces of sepiolite and montmorillonite. Appl. Clay Sci. 2020, 197, 105774.

Braga, S.S., 2019. Cyclodextrins: Emerging Medicines of the New Millennium. Biomolecules. 9, 801, 1-19.

Cheikh, D., Majdoub, H., Darder, M., 2022. An overview of clay-polymer nanocomposites containing bioactive compounds for food packaging applications. Appl. Clay Sci. 216, 106335.

de Breij, A., Karnaoukh, T.G., Schrumpf, J., Hiemstra, P.S., Nibbering, P.H., van Dissel, J.T., de Visser, P.C., 2016. The licorice pentacyclic triterpenoid component 18β-glycyrrhetinic acid enhances the activity of antibiotics against strains of methicillin-resistant Staphylococcus aureus. Eur. J. Clin. Microbiol. Infect. Dis. 35, 555–562.

Demirci, S., Sutekin, S.D., Sahiner, N. Polymeric Composites Based on Carboxymethyl Cellulose Cryogel and Conductive Polymers: Synthesis and Characterization, J. Compos. Sci. 4 (2020) 33.

Devi, N., Dutta, J., 2017. Preparation and characterization of chitosan-bentonite nanocomposite films for wound healing application. Int. J. Biol. Macromol. 104, 1897-1904.

Dian, L., Yu, E., Chen, X., Wen, X., Zhang, Z., Qin, L., Wang, Q., Li, G., Wu, C., 2014. Enhancing oral bioavailability of quercetin using novel soluplus polymeric micelles. Nanoscale Res. Lett. 9(684), 1-11.

Dorigato, A., Canclini, P., Unterberger, S.H., Pegoretti, A., 2017. Phase changing nanocomposites for low temperature thermal energy storage and release. Express Polym. Lett. 11 (9), 738-752.

Dorigato, A., Dzenis, Y., Pegoretti, A., 2013. Filler aggregation as a reinforcement mechanism in polymer nanocomposites. Mech. Mater. 61, 79-80.

EMA, 2017. Committee for Human Medicinal Products (CHMP). Cyclodextrins used as excipients. Report published in support of the 'Questions and answers on cyclodextrins used as excipients in medicinal products for human use' (EMA/CHMP/495747/2013).

Design and characterization of spring water hydrogels with natural inorganic excipients

García-Villén F., Sánchez-Espejo, R., López-Galindo, A., Cerezo P.,Viseras C., 2020. Design and

characterization of spring water hydrogels with natural inorganic excipients. Appl. Clay Sci. 1971, 105772.

Ghadiri, M., Chrzanowski, W., Rohanizade, R. 2015. Biomedical applications of cationic clay minerals. RSC Adv., 5, 29467-29481.

Ghasemiyeh, P., Samani, S.M., 2020. Potential of Nanoparticles as Permeation Enhancers and Targeted Delivery Options for Skin: Advantages and Disadvantages. Drug Des. Devel. Ther. 14, 3271-3289.

Giri, B.R., Kwon, J., Vo, A.Q., Bhagurkar, A.M., Bandari, S., Kim, D.W., 2021. Hot-melt extruded amorphous solid dispersion for solubility, stability, and bioavailability enhancement of telmisartan. Pharmaceuticals 14(1), 73.

Guo, F., Aryana, S., Han, Y., Jiao, Y. 2018. A Review of the Synthesis and Applications of Polymer–Nanoclay Composites. Appl. Sci. 8, 1696.

Konta, J., 1995. Clay and man: clay raw materials in the service of man. Appl. Clay Sci. 10(4), 275-335.

Jicsinszky, L., Cravotto, G., 2019. Cyclodextrins in Skin Formulations and Transdermal Delivery. J. Skin Stem. Cell. 6(4), e102561.

Kanikireddy, V., Varaprasad, K., Jayaramudu, T., Karthikeyan, C., Sadiku, R., 2020. Carboxymethyl cellulose-based materials for infection control and wound healing: A review. Int. J. Biol. Macromol. 164(1), 963-975

Kurakula, M., Rao, G.S.N.K., 2020. Pharmaceutical assessment of polyvinylpyrrolidone (PVP): As excipient from conventional to controlled delivery systems with a spotlight on COVID-19 inhibition. J. Drug Deliv. Sci. Technol. 60, 102046.

Lan, Y., Ali, S., Langley, N., 2010. Characterization of Soluplus® by FTIR and Raman Spectroscopy Results and Disscusion. CRS 2010 Annu. Conf.

Lin, H., Chi, Y.-T., Huang, Y.-T., Kao, C.-Y., Lin, S.-Y., 2015. DSC-FTIR Combined Approaches Used to Simultaneously Prepare/Determine the Amorphous Solid Dispersions of Indomethacin/Soluplus in Real-time. Pharm. Sci. 2.1, 183-193.

Massaro, M. Giuseppe Colletti, C., Lazzara, G., Riela S., 2018. The Use of Some Clay Minerals as Natural Resources for Drug Carrier Applications. J. Funct. Biomater. 9(4), 58.

Osman, A.F., Ashafee, A.M.T.L., Adnan, S.A., Alakrach, A., 2020. Influence of Hybrid Cellulose/Bentonite

Fillers on Structure, Ambient, and Low Temperature Tensile Properties of Thermoplastic Starch Composites. Polym. Eng. Sci. 60(4), 810-822.

Oyama, K., Kawada-Matsuo, M., Oogai, Y., Hayashi, T., Nakamura, N., Komatsuzawa, H., 2016. Antibacterial Effects of Glycyrrhetinic Acid and Its Derivatives on Staphylococcus aureus. PLoS One 11, e0165831.

Pagano, C., Ceccarini, M.R., Calarco, P., Scuota, S., Conte, C., Primavilla, S., Ricci, M., Perioli, L., 2019. Bioadhesive polymeric films based on usnic acid for burn wound treatment: Antibacterial and cytotoxicity studies. Colloids Surf. B Biointerfaces 178, 488–499.

Pagano, C., Marinozzi, M., Baiocchi, C., Beccari, T., Calarco, P., Ceccarini, M.R., Chielli, M., Orabona, C., Orecchini, E., Ortenzi, R., Ricci, M., Scuota, S., Tiralti, M.C., Perioli, L., 2020. Bioadhesive Polymeric Films Based on Red Onion Skins Extract for Wound Treatment: An Innovative and Eco-Friendly Formulation. Molecules 25(2), 318.

Paredes, A.J., McKenna, P.E., Ramöller, I.K., Naser, Y.A., Volpe-Zanutto, F., Li, M., Abbate, M.T.A., Zhao, L., Zhang, C., Abu-Ershaid, J.M., Dai, X., Donnelly, R.F., 2021. Microarray Patches: Poking a Hole in the Challenges Faced When Delivering Poorly Soluble Drugs. Adv. Funct. Mater. 31(1), 2005792.

Pellati, D., Fiore, C., Armanini, D., Rassu, M., Bertoloni, G., 2009. In vitro effects of glycyrrhetinic acid on the growth of clinical isolates of Candida albicans. Phyther. Res. 23, 572–574.

Peña-Parás, L., Sánchez-Fernández, J.A., Vidaltamayo, R. In: Handbook of Ecomaterials. Nanoclays for Biomedical Applications. L.M.T. Martínez et al. (eds.) Springer International Publishing AG 2018, pp. 1-19.

Peng, Q., Kong, D., Shi, L., Wang, X., Meng, X., Liu, N., 2020. Preparation of a novel bentonite intercalation composite by changing the chemical state of aluminum. J. Chinese Chem. Soc. 67(6), 1009-1015.

Perioli, L., Ambrogi, V., Angelici, F., Ricci, M., Giovagnoli, S., Capuccella, M., Rossi, C., 2004. Development of mucoadhesive patches for buccal administration of ibuprofen. J. Control. Release 99, 73–82.

Pignatello, R., Corsaro, R., 2019. Polymeric Nanomicelles of Soluplus® as a Strategy for Enhancing the Solubility, Bioavailability and Efficacy of Poorly Soluble Active Compounds. Curr. Nanomedicine 9(3), 184 - 197.

Ritger, P.L.; Peppas, N.A., 1987. A simple equation for description of solute release II. Fickian and anomalous

release from swellable devices. J. Control Release 5, 37-42.

Ryu, H.-J., Hang, N.T., Lee, J.-H., Choi, J.Y., Choi, G., Choy, J.-H., 2020. Effect of organo-smectite clays on the mechanical properties and thermal stability of EVA nanocomposites. Appl. Clay Sci. 196, Article 105750.

Saha, A.K., Dey Ray, S., 2013. Effect of cross-linked biodegradable polymers on sustained release of sodium diclofenac-loaded microspheres, Braz. J. Pharm. Sci. 49, 873-888.

Salehpour, S., Dubé, M.A., 2012. Reaction Monitoring of Glycerol Step-Growth Polymerization Using ATR-FTIR Spectroscopy. Macromol. React. Eng. 6 (2-3), 85-92.

Shamma, R.N., Basha, M., 2013. Soluplus®: A novel polymeric solubilizer for optimization of Carvedilol solid dispersions: Formulation design and effect of method of preparation. Powder Technol. 237, 406–414.

Shi, N.Q., Lai, H.W., Zhang, Y., Feng, B., Xiao, X., Zhang, H.M., Li, Z.Q., Qi, X.R., 2018. On the inherent properties of Soluplus and its application in ibuprofen solid dispersions generated by microwave-quench cooling technology. Pharm. Dev. Technol. 23(6), 1-48.

Siepmann, J.; Peppas, N.A., 2011. Higuchi equation: Derivation, applications, use and misuse. Int. J. Pharm. 418, 6-12.

Solanki, N., Gupta, S.S., Serajuddin, A.T.M., 2018. Rheological analysis of itraconazole-polymer mixtures to determine optimal melt extrusion temperature for development of amorphous solid dispersion. Eur. J. Pharm. Sci. 111(1), 482-491.

Sui, X., Chu, Y., Zhang, J., Zhang, H., Wang, H., Liu, T., Han, C., 2020. The Effect of PVP Molecular Weight on Dissolution Behavior and Physicochemical Characterization of Glycyrrhetinic Acid Solid Dispersions. Adv. Polym. Technol. 2020, 1-13.

Tian, B., Ju, X., Yang, D., Kong, Y., Tang, X., 2020. Effect of the third component on the aging and crystallization of cinnarizine-soluplus® binary solid dispersion. Int. J. Pharm. 580, 119240.

Tsinman, O., Tsinman, K., Ali, S., 2015. Excipient update - soluplus®: An understanding of supersaturation from amorphous solid dispersions. Drug Dev. Deliv. 15(1), 1-11.

Ugoeze, K.C., 2020. Bioadhesive Polymers for Drug Delivery Applications, in: Bioadhesives in Drug Delivery, Mittal, K.L., Bakshi, I.S., Narang, J.K. (eds.), Scrivener Publishing, Beverly (MA), pp. 29-56.

Vipulanandan C., Mohammed A. 2020. Zero fluid loss, sensitivity and rheological properties of clay bentonite (WBM) modified with nanoclay quantified using Vipulanandan models. Upstream Oil and Gas Technol. 5, 100012.

Xu, Y., Zhang, Y., 2015. Synthesis of polypyrrole/sodium carboxymethyl cellulose nanospheres with enhanced supercapacitor performance, Mater. Lett. 139, 145-148.

Zeng, Y.C., Li, S., Liu, C., Gong, T., Sun, X., Fu, Y., Zhang, Z.R., 2017. Soluplus micelles for improving the oral bioavailability of scopoletin and their hypouricemic effect in vivo. Acta Pharmacol. Sin. 38(3), 424-433.

Zhu, T.T., Zhou, C.H., Kabwe, F.B., Wu, Q.Q., Li, C.S., Zhang, J.R., 2019. Exfoliation of montmorillonite and related properties of clay/polymer nanocomposites. Appl. Clay Sci. 169(596), 48-66.

Table 1

Compositions of hydrogels used to prepare patches prototypes.

Hydrogels	CMC (wt%)	PVP K90 (wt%)	BE (wt%)	NC (wt%)	SL (wt%)	Glycerol (wt%)	Water (wt%)
H - CMC_S_1	3.0	0.1	–	–	1.0	10	85.9
H - CMC_BE_0.5	3.0	0.1	0.5	–	0.5	10	85.9
H - CMC_BE_0.7	3.0	0.1	0.7	–	0.3	10	85.9
H - CMC_BE_1	3.0	0.1	1.0	–	–	10	85.9
H - CMC_NC_0.5	3.0	0.1	–	0.5	0.5	10	85.9
H - CMC_NC_0.7	3.0	0.1	–	0.7	0.3	10	85.9
H - CMC_NC_1	3.0	0.1	–	1.0	–	10	85.9
H - CMC_S_0	3.0	0.1	–		–	10	86.9

Table 2

Main results of quasi static tensile tests and creep tests: secant moduli at deformations of 5% ($E_{5\%}$), 25% ($E_{25\%}$) and 50% ($E_{50\%}$), stress at break (σ_b), deformation at break (ε_b), and creep compliance at 60 min.

Patch	Thickness (mm)	E5% (MPa) ± SD	E25% (MPa) ± SD	E50% (MPa) ± SD	σ_b (MPa) ± SD	ε_b (%) ± SD	Creep compliance (t = 60 min) [MPa^{-1}]
CMC_S_1	0.2010 ± 0.030	0.034 ± 0.010	0.023 ± 0.003	0.023 ± 0.002	0.029 ± 0.009	364 ± 13	50.80
CMC_BE_0.5	0.4704 ± 0.012	0.071 ± 0.012	0.050 ± 0.006	0.051 ± 0.006	0.051 ± 0.008	383 ± 53	28.32
CMC_BE_0.7	0.4979 ± 0.023	0.164 ± 0.064	0.104 ± 0.034	0.093 ± 0.027	0.069 ± 0.025	411 ± 11	26.00
CMC_BE_1	0.5564 ± 0.031	0.162 ± 0.064	0.120 ± 0.043	0.113 ± 0.040	0.096 ± 0.075	427 ± 81	14.74
CMC_NC_0.5	0.3422 ± 0.042	0.081 ± 0.031	0.056 ± 0.015	0.054 ± 0.015	0.064 ± 0.015	404 ± 40	26.88
CMC_NC_0.7	0.4268 ± 0.051	0.053 ± 0.035	0.054 ± 0.019	0.054 ± 0.020	0.044 ± 0.016	316 ± 50	28.45
CMC_NC_1	0.2508 ± 0.018	0.070 ± 0.040	0.090 ± 0.013	0.088 ± 0.014	0.075 ± 0.042	414 ± 61	8.15
CMC_S_0	0.4186 ± 0.079	0.045 ± 0.013	0.033 ± 0.004	0.031 ± 0.004	0.033 ± 0.016	394 ± 32	51.44

Table 3

Content of Gly in the patches measured sperimentally; thermal data and creep compliace of unloaded and loaded patches.

Patch	Experimental content mg/cm^2 (±SD)	T_d (°C)	% H_2O (120 °C) (wt%)	Residual mass (wt%)	T_g (°C)	H_2O (wt%)	Creep compliance unloaded patches (t = 60 min) (MPa^{-1})	Creep compliance loaded patches (t = 60 min) (MPa^{-1})
CMC_BE_0.5	0.44 ± 0.01	175.8	27.0	7.0	143.9	29.3	28.32	32.8
CMC_BE_1	0.42 ± 0.02	175.5	26.7	8.7	120.6	29.9	14.74	18.2
CMC_NC_0.5	0.42 ± 0.02	173.7	24.2	7.8	116.2	28.4	26.88	31.6
CMC_NC_1	0.43 ± 0.03	174.9	23.8	10.0	109.4	27.1	8.15	25.7

Table 4

Equations and R^2 values obtained by the application of the kinetic mathematical models (zero-order, Higuchi, first-order).

Patch	$M_t/M_\infty = kt$	$M_t/M_\infty = kt^{0.5}$	$M_t/M_\infty = 1-e^{-kt}$
	Zero-order kinetic	Higuchi kinetic (release 0–60%)	First order kinetic
CMC_BE_0.5 Gly	y = 0.0132× + 38.594	y = 2.1887× + 18.186	y = −0.0002 × −0.187
	R^2 = 0.53	R^2 = 0.88	R^2 = 0.63
CMC_NC_0.5 Gly	y = 0.0284× + 24.151	y = 1.4111× + 13.837	y = −0.0005 × −0.0817
	R^2 = 0.85	R^2 = 0.64	R^2 = 0.96

M∞: amount of drug at the equilibrium state; Mt.: amount of drug released over time t, k: release velocity constant; n: exponent of release (related to the drug release mechanism) in function of time t; e: Euler's number.

Table 5

Results of the antimicrobial activity of the two loaded patches.

S. aureus WDCM 00034			
Time (h)	Control	CMC_BE_0.5_Gly	CMC_NC_0.5_Gly
	Log CFU/ml	Log CFU/ml	Log CFU/ml
0	3.51	3.51	3.51
6	6.51	4.45	3.71
24	7.93	7.04	6.20
MRSA ATCC BAA-1708			
0	3.45	3.45	3.45
6	5.62	4.90	4.86
24	7.86	7.43	7.60

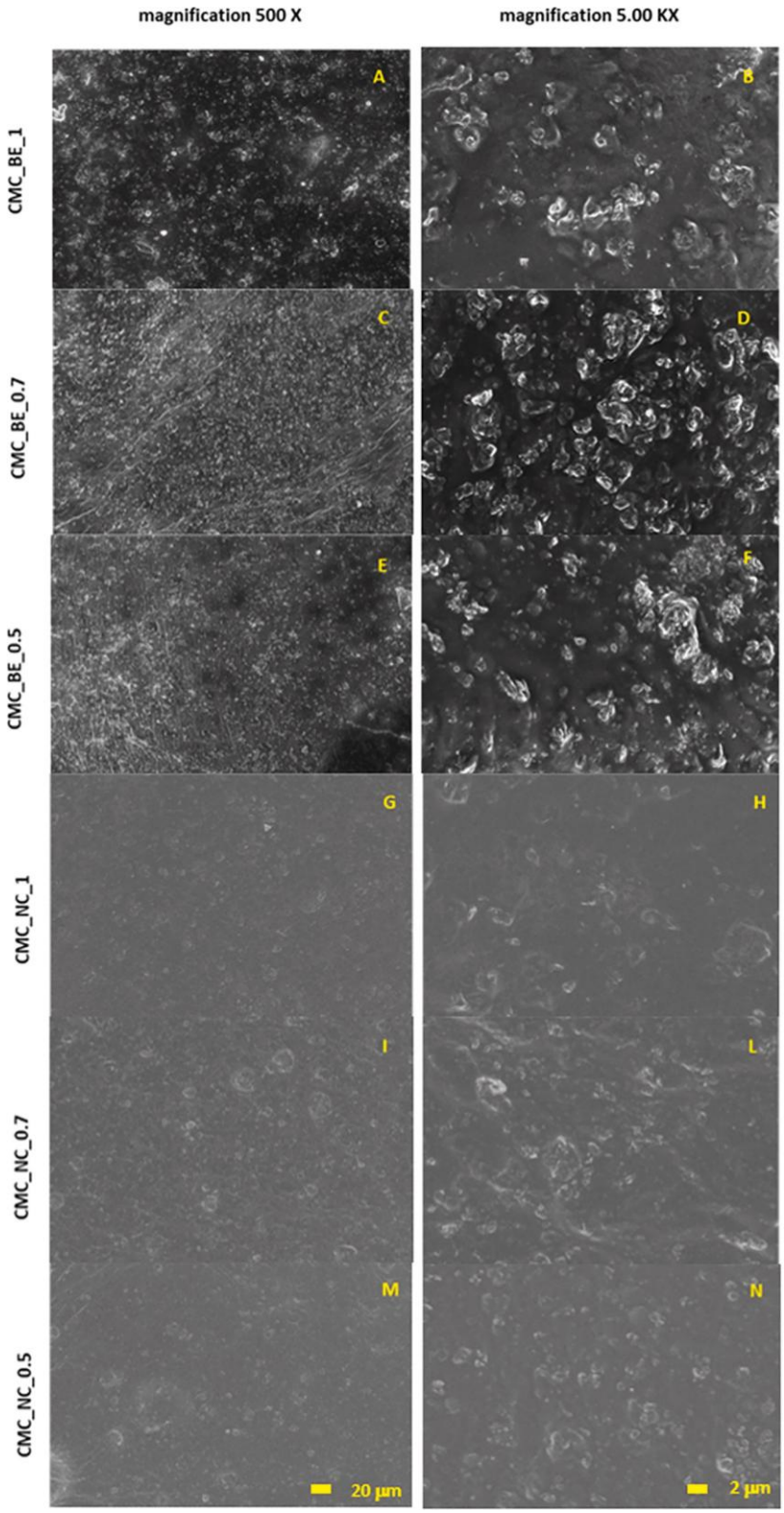

Fig. 1. Micrographs of CMC_BE_1 (A, B); CMC_BE_0.7 (C, D); CMC_BE_0.5 (E, F); CMC_NC_1 (G, H); CMC_NC_0.7 (I, L); CMC_NC_0.5 (M, N).

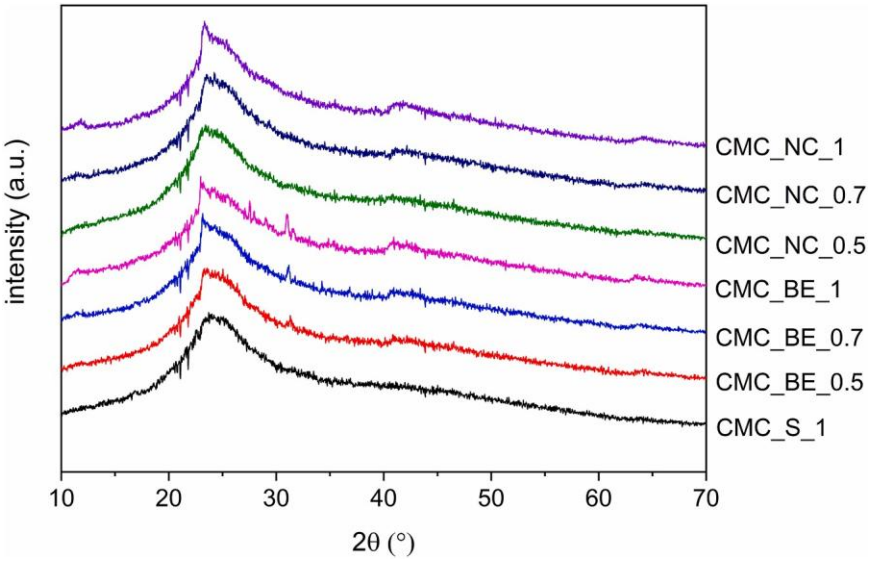

Fig. 2. XRD diffractograms of the dried patches.

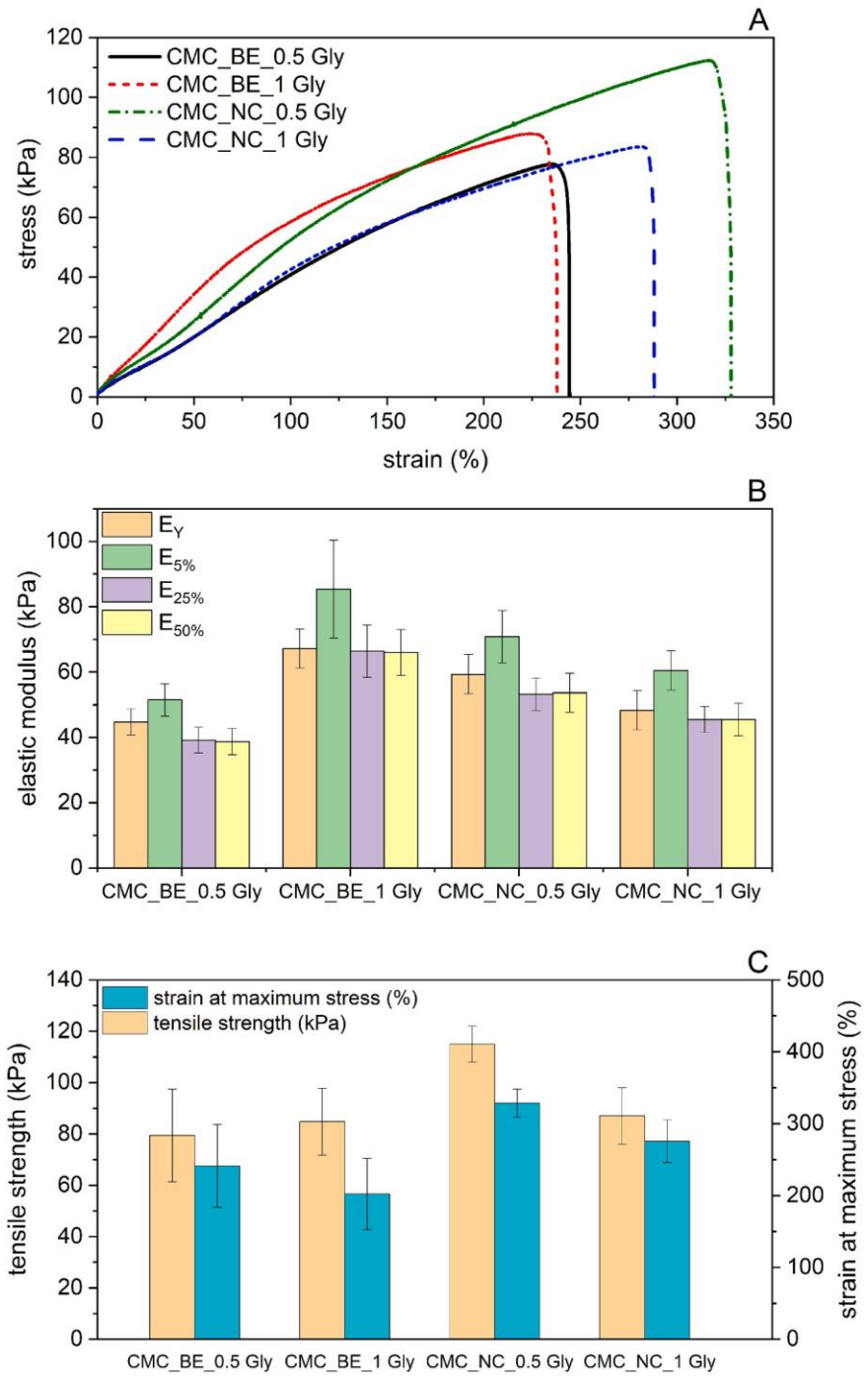

Fig. 3. Main results of the quasi static tensile tests on the loaded samples. (A) representative stress-strain curves; (B) values of elastic modulus (E_Y, $E_{5\%}$, $E_{25\%}$, $E_{50\%}$) and (C) tensile strength (maximum stress) and corresponding strain for the four tested samples.

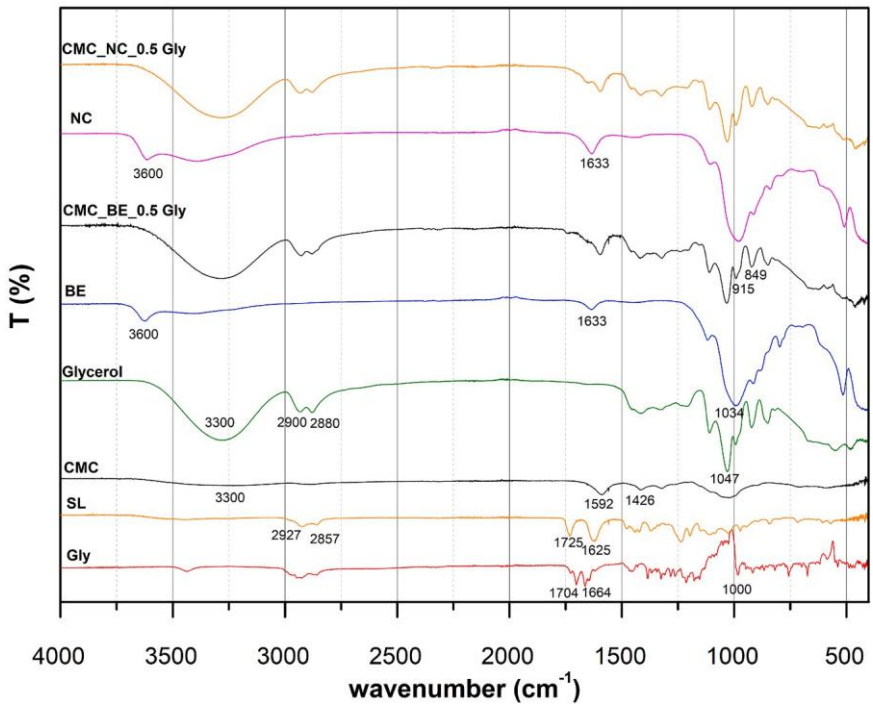

Fig. 4. FT-IR spectra registered for: the raw materials crystalline Gly, SL, CMC, glycerol, Bent (NC and BE) and for the loaded patches CMC_NC_0.5_Gly and CMC_BE_0.5_Gly.

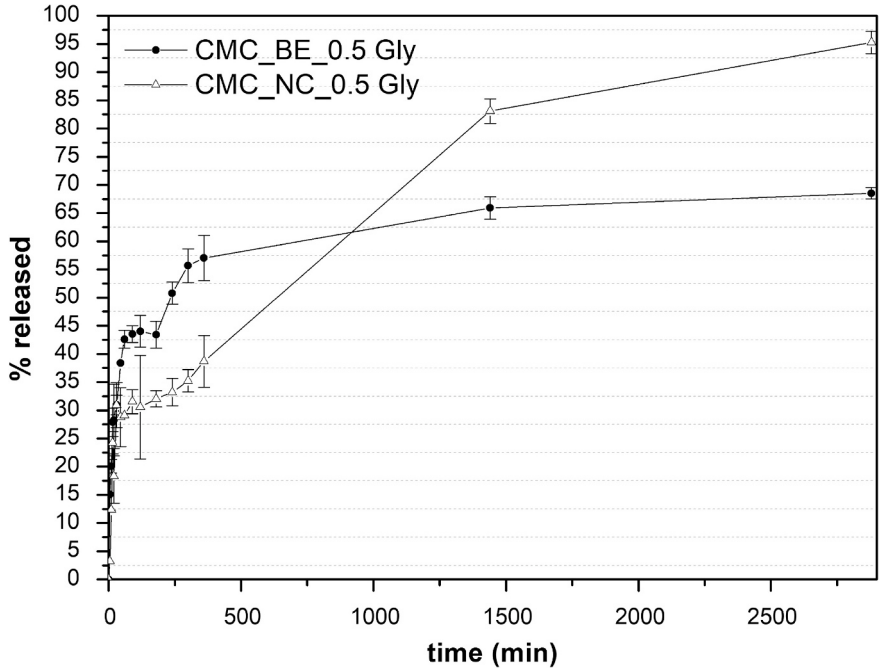

Fig. 5. Release profiles of Gly from CMC_BE_0.5 Gly and CMC_NC_0.5_Gly patches (circle of 3.14 cm^2) obtained in vitro by vertical Franz diffusion cell using EtOH/ SWF (50/50) solution pH 6.5 at 32 °C as acceptor medium ($n = 3$, ±SD).